Mechanics of Advanced Composite Structures 2 (2014) 113 – 130

Semnan University

Mechanics of Advanced Composite Structures

journal homepage: http://MACS.journals.semnan.ac.ir

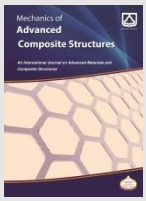

A Semi-analytical Solution for 3-D Dynamic Analysis of Thick Continuously Graded Carbon Nanotube-reinforced Annular Plates Resting on a Two-parameter Elastic Foundation

V. Tahouneh*[a], J. Eskandari- Jam [b]

[a] *Department of Mechanical Engineering, Islamshahr Branch, Islamic Azad University, Tehran, Iran*
[b] *Composite Materials and Technology Center, Tehran, Iran*

PAPER INFO

Paper history:
Received 30 July 2014
Received in revised form 16 November 2014
Accepted 21 November 2014

Keywords:
Three-dimensional free vibration
Continuously graded carbon nanotube-reinforced
Annular plates
Two-parameter elastic foundations

ABSTRACT

The The main objective of this research paper is to present 3-D elasticity solution for free vibration analysis of elastically supported continuously graded carbon nanotube-reinforced (CGCNTR) annular plates. The volume fractions of oriented, straight single-walled carbon nanotubes (SWCNTs) are assumed to be graded in the thickness direction. An equivalent continuum model based on the Eshelby-Mori-Tanaka approach is employed to estimate the effective constitutive law of the elastic isotropic medium (matrix) with oriented, straight carbon nanotubes (CNTs). A semi-analytical approach composed of 2-D differential quadrature method and series solution is adopted to solve the equations of motion. The novelty of the present work is to exploit Eshelby-Mori-Tanaka approach in order to reveal the impacts of the volume fractions of oriented CNTs and different CNTs distributions on the vibrational characteristics of CGCNTR annular plates.

1. Introduction

Recently, Recently, Nanocomposites have significant importance for engineering applications that require high levels of structural performance and multifunctionality. Carbon Nanotubes (CNTs) have demonstrated exceptional mechanical, thermal and electrical properties. These materials are considered as one of the most promising reinforcement materials for high-performance structural and multifunctional composites with vast application potentials [1]. A detailed summary of the mechanical properties of CNTs can be found in [2]. The exceptional mechanical properties of CNTs have shown great promise for a wide variety of applications, such as nanotransistors, nanofillers, semiconductors, hydrogen storage devices, structural materials, molecular sensors, field-emission-based displays, and fuel cells [3]. The addition of nano-sized fibers or nanofillers, such as CNTs, can further increase the merits of polymer composites [4]. These nanocomposites, easily processed due to the small diameter of the CNTs, exhibit unique properties [5,6], such as enhanced modulus and tensile strength, high thermal stability and good environmental resistance. This behavior, combined with their low density makes CNTs suitable for a broad range of technological sectors such as telcommunications, electronics [7] and transport

* Corresponding author. Tel.: +98-21-22935300, Fax: +98-21-22936578

E-mail address: jejam@mail.com (J.Eskandari- Jam).

dustries, especially for aeronautic and aerospace applications where the reduction in weight is crucial in order to reduce the fuel consumption. For example, Qian et al. [8] showed that the addition of 1 wt.% (i.e. 1% by weight) multiwall CNT to polystyrene resulted in 36-42% and ~25% increase in the elastic modulus and the break stress of the nanocomposite properties, respectively. In addition, Yokozeki et al. [9] reported the retardation of the onset of matrix cracking in the composite laminates containing the cup-stacked CNTs compared to those without the cup-stacked CNTs. Most studies on CNT-Reinforced Composites (CNTRCs) have focused on their material properties [10–14]. Shen [15] for the first time suggests that the nonlinear bending behavior can be considerably improved through the use of a functionally graded distribution of CNTs in the matrix. He introduced the CNT efficiency parameter to account load transfer between the nanotube and polymeric phases. Compressive postbuckling and thermal buckling behavior of functionally graded nanocomposite plates reinforced by aligned, straight Single-Walled CNTs (SWCNTs) subjected to in-plane temperature variation was reported by Shen and Zhu [16] and Shen and Zhang [17]. They find that in some cases the CNTRC plate with intermediate CNT volume fraction does not have intermediate buckling temperature and initial thermal postbuckling strength. Moreover, Ke et al. [18] investigated the nonlinear free vibration of functionally graded CNTRC Timoshenko beams. They find that both linear and nonlinear frequencies of functionally graded CNTRC beam with symmetrical distribution of CNTs are higher than those of beams with uniform or unsymmetrical distribution of CNTs. To the best of authors' knowledge the review of open literature showed that the studies on functionally graded CNTRCs were restricted to nanocomposite structures having graded aligned, straight CNTs in the thickness direction, and effective material properties of CNTRCs were estimated through the extended rule of mixture. This fact motivates us to employ the Eshelby-Mori-Tanaka approach for calculating the elastic stiffness properties of nanocomposite materials reinforced by graded oriented, straight CNTs. Plates resting on elastic foundations have found considerable applications in structural engineering problems. Reinforced-concrete pavements of highways, airport runways, foundation of storage tanks, swimming pools, and deep walls together with foundation slabs of buildings are well-known direct applications of these kinds of plates. The underlying layers are modeled by a Winkler-type elastic foundation. The most serious deficiency of the Winkler foundation model is having no interaction between the springs. In other words, the springs in this model are assumed to be independent and unconnected. The Winkler foundation model is fairly improved by adopting the Pasternak foundation model, a two-parameter model, in which the shear stiffness of the foundation is considered. A closed-form solution for the vibration frequencies of simply supported Mindlin plates on Pasternak foundations and subjected to biaxial initial stresses was presented by Xiang et al. [19]. The buckling load of Mindlin plates on Pasternak foundations was obtained in terms of the thin plate solution. Based on first-order shear deformation plate theory, the buckling and vibration analysis of moderately thick laminates on Pasternak foundations was presented by Xiang et al. [20]. The effects of foundation parameters, transverse shear deformation, and rotary inertia and the number of layers on the buckling and vibration of cross-ply laminates were examined. Wang et al. [21] presented relationships between the buckling loads of simply supported plates on a Pasternak foundation determined by classical Kirchhoff plate theory, Reissner–Mindlin plate theory, and Reddy plate theory. The vibration of polar orthotropic circular plates on an elastic foundation was investigated by Gupta et al. [22]. The Mindlin shear deformable plate theory was employed and the Chebyshev collocation method was applied to obtain the frequency parameters of the circular plates. Ju et al. [23] developed a finite element model to study the vibration of Mindlin plates with multiple stepped variations in thickness and resting on non-homogeneous elastic foundations. Gupta et al. [24,25] studied the effect of elastic foundation on axisymmetric vibrations of polar orthotropic circular plates of variable thickness by taking approximating polynomials in Rayleigh–Ritz method. Laura and Gutierrez [26] analyzed the free vibration of a solid circular plate of linearly varying thickness attached to Winkler foundation using the Ritz method. Matsunaga [27] analyzes the natural frequencies and buckling stresses of FG plates using a higher order shear deformation theory which are based on the through the thickness series expansion of the displacement components. Zhou et al. [28] used Ritz method to analyze the free-vibration characteristics of rectangular thick plates resting on elastic foundations. Matsunaga [29] investigated a two-dimensional, higher-order theory for analyzing the thick simply supported rectangular plates resting on elastic foundations. Tahouneh and Yas [30] investigated the free vibration analysis of thick FG annular sector plates on Pasternak elastic foundations using DQM. Tahouneh and Yas [31] studied free vibration characteristics of thick multi-directional functionally graded annular sector plates under various boundary condition using 2-D differential quadrature method. They show that a graded ceramic volume frac-

tion in two directions has a higher capability to reduce the natural frequency than conventional 1-D FGM. Tahouneh et al. [32] investigated the effect of continuous grading fiber reinforced on the vibrational response of thick annular plates using DQ method. More recently, Tahouneh [33] studied the three-dimensional free vibration analysis of Continuous Grading Fiber Reinforced (CGFR) sector plates with simply supported radial edges and arbitrary boundary conditions on their circular edges using 2D DQ method. Jam et al. [34] studied free vibrations of three-parameter functionally graded plates resting on Pasternak foundations using GDQ method. Nie and Zhong [35] investigated three-dimensional vibration of FG circular plates using semi-analytical method. Dong [36] developed a three-dimensional free vibration analysis of FG annular plates using the Chebyshev-Ritz method. Cheng and Batra [37] used Reddy's third-order plate theory to study steady state vibrations and buckling of a simply supported functionally gradient isotropic polygonal plate resting on a Pasternak elastic foundation and subjected to uniform in-plane hydrostatic loads. Malekzadeh [38] studied free vibration analyses of functionally graded plates on elastic foundations based on the three-dimensional elasticity. In structural mechanics, one of the most popular semi-analytical methods is Differential Quadrature Method (DQM) [39], remarkable success of which is demonstrated by many researchers in vibration analysis of plates, shells, and beams. Liu and Liew [40], and Liew and Liu [41] presented DQM for free vibration analysis of Mindlin isotropic circular and annular sector plates with various types of boundary conditions. A new version of the DQM was extended by Wang and Wang [42] to analyze the free vibration of thin circular sector plates with six combinations of boundary conditions. Liew et al. [43] employed DQM for free vibration analysis of moderately thick plates on Winkler foundation. Gupta et al. [44] studied the free vibration analysis of non-homogeneous circular plate of nonlinear thickness variation using the DQM. Nie and Zhong [45] studied the free vibration of FG plates without elastic foundation using DQM. They assume the material properties of the FG plate have an exponent-law variation along the thickness, radial direction or both directions. The mathematical fundamental and recent developments of differential quadrature method as well as its major applications in engineering are discussed in detail in the book by Shu [46].This paper is motivated by the lack of studies in the technical literature concerning to the three-dimensional vibration analysis of a Continuously Graded Carbon Nanotube-Reinforced (CGCNTR) annular plates resting on a two-parameter foundation. To the authors' best knowledge, research on the vibration of thickness a continuously graded carbon nanotube-reinforced (CGCNTR) annular plates resting on a two-parameter foundation based on the three-dimensional theory of elasticity has not been seen yet. In this study, the volume fractions of oriented, straight Single-Walled Carbon Nanotubes (SWCNTs) are assumed to be graded in the thickness direction. An equivalent continuum model based on the Eshelby-Mori-Tanaka approach is employed to estimate the effective constitutive law of the elastic isotropic medium (matrix) with dispersed elastic inhomogeneities (oriented CNTs). A sensitive analysis is performed, and the natural frequencies are calculated for different sets of boundary conditions and different combinations of the geometric, and foundational parameters. Therefore, very complex combinations of the material properties, boundary conditions, and foundation stiffness are considered in the present semi-analytical solution approach.

2. Problem Description

The geometric configuration of a CGCNTR annular thick plate is shown in Fig. 1. a, b and h are outer/inner radius and thickness of the plate, respectively. The plate is supported by an elastic foundation with Winkler's (normal) and Pasternak's (shear) coefficients. The deformations defined with reference to a cylindrical coordinate system(r, θ, z) are u_r ,u_θ and u_z in the r , θ and z directions, respectively. We assume that the CGCNTR annular plate is made of a mixture of oriented, straight SWCNT, graded distribution in the thickness direction, and polymer matrix which is assumed to be isotropic [47].

2.1. Estimation of Effective Material Properties of CNTRC

In this study, we exploit an equivalent continuum model based on the Eshelby-Mori-Tanaka approach in order to estimate the effective constitutive law of the elastic isotropic medium (matrix) with dispersed elastic inhomogeneities (carbon nanotubes). The major step towards modeling materials with fully dispersed inhomogeneities was taken by Mori and Tanaka [48]. In particular, the presence of multiple inclusions and boundary conditions and their interactions are accounted by them. Giordano et al. [49] used the homogenization procedure, based on the Eshelby theory, under small deformations and small volume fractions of the embedded phases, to determine the bulk and shear moduli and Landau coefficients of the composite material. Previous studies have established the validity of the Eshelby-Mori-Tanaka approach in determining the effective properties of composites reinforced with misaligned,

carbon fibres, and with carbon nanotubes [14,50,51]. In this paper, the proposed model is framed with the Eshelby theory for elastic inclusions. The original theory of Eshelby [52,53] is restricted to one single inclusion in a semi-infinite elastic, homogeneous and isotropic medium. The theory, generalized by Mori-Tanaka, allows extending the original approach to the practical case of multiple inhomogeneities embedded into a finite domain. The Eshelby-Mori-Tanaka approach, based on the equivalent elastic inclusion idea of Eshelby and the concept of average stress in the matrix according to Mori-Tanaka, is also known as the equivalent inclusion-average stress method [54].

2.1.1. Nanocomposite Reinforced by Aligned, Straight CNTs

a linear elastic polymer matrix reinforced by a large number of dispersed straight CNTs is considered. First, we consider a polymer composite reinforced with aligned and straight CNTs. According to Benveniste'srevisitation [50], the following equation of the effective elastic tensor is obtained:

$$C = C_m + f_r\langle (C_r - C_m)A_r\rangle (f_m I + f_r\langle A_r\rangle)^{-1} \quad (1)$$

Where f_r and f_m are the fiber and matrix volume fractions, respectively, I is the identity tensor, C_m is the stiffness tensor of the matrix material, C_r is the stiffness tensor of the equivalent fiber, and A_r is the dilute mechanical strain concentration tensor for the fiber which is obtained through the following formula:

$$A_r = \left[I + S(C_m)^{-1}(C_r - C_m) \right]^{-1} \quad (2)$$

The tensor S is Eshelby's tensor, as given by Eshelby [52] and Mura [55]. The terms enclosed with angle brackets in Eq. (1) represent the average value of the term over all orientations defined by transformation from the local fiber coordinates $(o - \acute{x}_1\acute{x}_2\acute{x}_3)$ to the global coordinates$(o - x_1x_2x_3)$, as it is shown in Fig. 2. The matrix is assumed to be elastic and isotropic, with Young's modulus E_m and Poisson's ratio υ_m. Each straight CNT is modeled as a long fiber with transversely isotropic elastic properties. Therefore, the composite is also transversely isotropic. The substitution of non-vanishing components of the Eshelby tensor S for a straight, long fiber along the x_2- direction in Eq. (2) gives the dilute mechanical strain concentration tensor. Then inserting A_r into Eq. (1) gives the tensor of effective elastic moduli of the composite reinforced by aligned and straight CNTs.

In particular, the Hill's elastic moduli are found as [47]:

$$k = \frac{E_m\{E_m f_m + 2k_r(1+\upsilon_m)[1+f_r(1-2\upsilon_m)]\}}{2(1+\upsilon_m)[E_m(1+f_r-2\upsilon_m)+2f_m k_r(1-\upsilon_m-2\upsilon_m^2)]} \quad (3)$$

$$l = \frac{E_m\{\upsilon_m f_m[E_m+2k_r(1+\upsilon_m)]+2f_r k_r(1-\upsilon_m^2)\}}{(1+\upsilon_m)[E_m(1+f_r-2\upsilon_m)+2f_m k_r(1-\upsilon_m-2\upsilon_m^2)]} \quad (4)$$

$$m = \frac{E_m^2 f_m(1+f_r-f_m\upsilon_m)+2f_m f_r(k_r n_r - l_r^2)(1+\upsilon_m)^2(1-2\upsilon_m)}{(1+\upsilon_m)[E_m(1+f_r-2\upsilon_m)+2f_m k_r(1-\upsilon_m-2\upsilon_m^2)]} + \frac{E_m[2f_m^2 k_r(1-\upsilon_m)+f_r n_r(1+f_r-2\upsilon_m)-4f_m l_r\upsilon_m]}{E_m(1+f_r-2\upsilon_m)+2f_m k_r(1-\upsilon_m-2\upsilon_m^2)} \quad (5)$$

$$n = \frac{E_m[E_m f_m + 2p_r(1+\upsilon_m)(1+f_r)]}{2(1+\upsilon_m)[E_m(1+f_r)+2f_m p_r(1+\upsilon_m)]} \quad (6)$$

$$p = \frac{E_m[E_m f_m + 2m_r(1+\upsilon_m)(3+f_r-4\upsilon_m)]}{2(1+\upsilon_m)\{E_m[f_m+4f_r(1-\upsilon_m)]+2f_m m_r(3-\upsilon_m-4\upsilon_m^2)\}} \quad (7)$$

Where *k, l, m, n*, and *p* are Hill's elastic moduli of the composite; k is the plane-strain bulk modulus normal to the fiber direction, *n* is the uniaxial tension modulus in the fiber direction, *l* is the associated cross modulus, *m* and *p* are the shear moduli in planes normal and parallel to the fiber direction, respectively. In addition, k_r,l_r , m_r ,n_r , and p_r are the Hill's elastic moduli for the reinforcing phase (CNTs). The elastic moduli parallel and normal to CNTs are related to Hill's elastic moduli through what follows:

$$E_{\parallel} = n - \frac{l^2}{k} \quad , E_{\perp} = \frac{4m(kn-l^2)}{kn-l^2+mn} \quad (8)$$

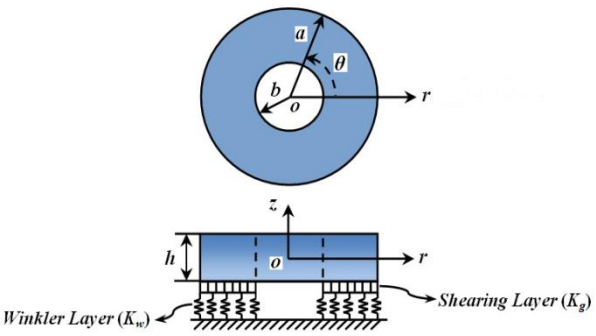

Figure 1. The sketch of an elastically supported thick continuously graded carbon nanotube reinforced annular plate and setup of the coordinate system.

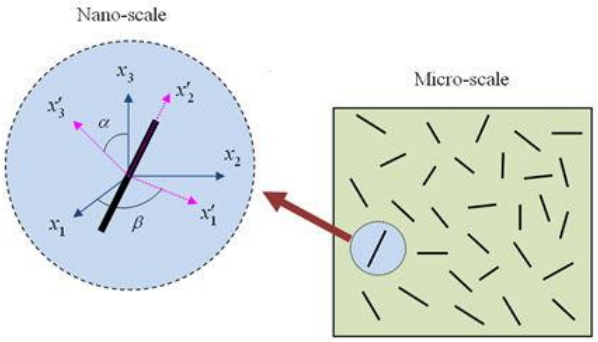

Figure 2. Representative volume element (RVE) including straight CNTs.

2.1.2. Nanocomposite Reinforced by Oriented, Straight CNTs

In this section, the influence of oriented, straight CNTs is investigated. The orientation of a straight CNT is characterized using two Euler angles α and β, as shown in Figure 2. The orientation distribution of CNTs in the CNTRC is characterized using a probability density function for oriented nanotubes in which case the composite is isotropic. The base vectors e_i and $\acute{e}_i$ of the global $(o - x_1x_2x_3)$ and the local coordinate systems $(o - \acute{x}_1\acute{x}_2\acute{x}_3)$ are related via the transformation matrix g as follows:

$$e_i = g_{ij}e'_j \tag{9}$$

Where g is given by

$$g = \begin{bmatrix} \cos\beta & -\cos\alpha\sin\beta & \sin\alpha\sin\beta \\ \sin\beta & \cos\alpha\cos\beta & -\sin\alpha\cos\beta \\ 0 & \sin\alpha & \cos\alpha \end{bmatrix} \tag{10}$$

The orientation distribution of CNTs in a composite is characterized using a probability density function P(α, β) satisfying the normalization condition as the following [47]:

$$\int_0^{2\pi}\int_0^{\pi/2} p(\alpha,\beta)(\sin\alpha)d\alpha d\beta = 1 \tag{11}$$

If CNTs are completely oriented, the density function is the following:

$$p(\alpha,\beta) = 1/2\pi \tag{12}$$

According to the Mori-Tanaka method, the strain $\varepsilon_r(\alpha,\beta)$and the stress $\sigma_r(\alpha,\beta)$ of the CNT are related to the stress of matrix σ_m by the following equations:

$$\begin{aligned} &\varepsilon_r(\alpha,\beta) = A(\alpha,\beta)\varepsilon_m = A(\alpha,\beta)C_m^{-1}\sigma_m, \\ &\sigma_r(\alpha,\beta) = C_r A(\alpha,\beta)\varepsilon_m = [C_r A(\alpha,\beta)C_m^{-1}]\sigma_m \end{aligned} \tag{13}$$

Where the strain concentration tensor $A(\alpha,\beta)$ is given by Eq. 2. Then the average strain and stress in all oriented CNTs are written as the following:

$$\begin{aligned} &\langle\varepsilon_r\rangle = \left[\int_0^{2\pi}\int_0^{\pi/2} p(\alpha,\beta)A(\alpha,\beta)\sin\alpha d\alpha d\beta\right]\varepsilon_m, \\ &\langle\sigma_r\rangle = \left[\int_0^{2\pi}\int_0^{\pi/2} p(\alpha,\beta)\left[C_r A(\alpha,\beta)C_m^{-1}\right]\sin\alpha d\alpha d\beta\right]\sigma_m \end{aligned} \tag{14}$$

Using The angle brackets represent the average over special orientations. Using the average theorems $\sigma = f_m\sigma_m + f_r\langle\sigma_r\rangle$ and $\varepsilon = f_m\varepsilon_m + f_r\langle\sigma_r\rangle$ in conjunction with the effective constitutive relation $\sigma = C\varepsilon$, one can get the effective modulus of the composite according to Eq. (1). When CNTs are completely oriented in the matrix, the composite is then isotropic, and its bulk modulus *K* and shear modulus *G* are derived as what follows:

$$K = K_m + \frac{V_f(\delta_r - 3K_m\alpha_r)}{3(V_m - V_f\alpha_r)} \tag{15}$$

$$G = G_m + \frac{V_f(\eta_r - 2G_m\beta_r)}{2(V_m - V_f\beta_r)} \tag{16}$$

Where

$$\alpha_r = \frac{3(K_m + G_m) + k_r + l_r}{3(k_r + G_m)} \tag{17}$$

$$\begin{aligned} \beta_r = \frac{1}{5}\Bigg(&\frac{4G_m + 2k_r + l_r}{3(G_m + k_r)} + \frac{4G_m}{G_m + p_r} + \\ &\frac{2\left[G_m(3K_m + G_m) + G_m(3K_m + 7G_m)\right]}{G_m(3K_m + G_m) + m_r(3K_m + 7G_m)}\Bigg) \end{aligned} \tag{18}$$

$$\delta_r = \frac{1}{3}\left[n_r + 2l_r + \frac{(2k_r + l_r)(3K_m + 2G_m - l_r)}{G_m + k_r}\right] \tag{19}$$

$$\begin{aligned} \eta_r = &\frac{1}{5}\left[\frac{2}{3}(n_r - l_r) + \frac{8G_m p_r}{G_m + p_r} + \frac{2(k_r - l_r)(2G_m + l_r)}{3(G_m + k_r)}\right] + \\ &\frac{1}{5}\left[\frac{8m_r G_m(3K_m + 4G_m)}{3K_m(m_r + G_m) + G_m(7m_r + G_m)}\right] \end{aligned} \tag{20}$$

Where K_m and G_m are the bulk and shear moduli of the matrix, respectively. In addition, k_r, m_r, n_r and l_r are the Hill's elastic moduli for the reinforcing phase. The effective Young's modulus E and Poisson's ratio υ of the material are obtained using the following equations:

$$E = \frac{9KG}{3K + G} \tag{21}$$

$$\upsilon = \frac{3K - 2G}{6K + 2G} \tag{22}$$

In addition, V_f and V_m are the volume fractions of the CNTs and the matrix, which satisfy the relationship of $V_f + V_m = 1$ imilarly, mass density ρ is calculated using the following equation:

$$\rho = \rho_f V_f + \rho_m V_m \tag{23}$$

Where ρ_f and ρ_m are the mass density of the CNTs and the matrix, respectively. In order to examine the effect of different CNTs distribution on the free vibration characteristics of CGCNTR annular plates resting on elastic foundations, various types of material profiles are considered through the plate thickness $(\eta_z = z/h)$. In this work, we assume only linear distribution of CNTs volume fraction for the different types of the CGCNTR annular plate, as follow:

$$CGCNTR-\mathrm{V}: V_f = 2\left[\frac{z}{h}+0.5\right]V_f^* \tag{24}$$

$$CGCNTR-\Lambda: V_f = -2\left[\frac{z}{h}-0.5\right]V_f^* \tag{25}$$

$$CGCNTR-\mathrm{X}: V_f = 4\left[\frac{|z|}{h}\right]V_f^* \tag{26}$$

$$CGCNTR-\Diamond: V_f = 4\left[0.5-\frac{|z|}{h}\right]V_f^* \tag{27}$$

Where V_f^* is the volume fraction of CNTs [11,15,56] that is calculated by the mass fraction of nanotubes, m_f, assuming two phases and no trapped air, using the following equation [11]:

$$V_f^* = \left[\frac{\rho_r}{m_f} - \rho_r + 1\right]^{-1} \tag{28}$$

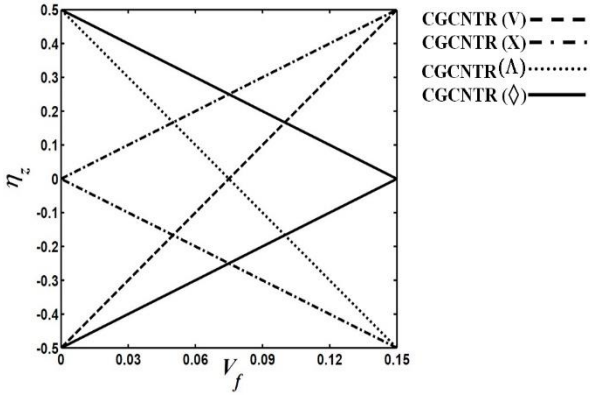

Figure 3. Variations of CNTs volume fractions through the thickness of the plate for different types of CNT distribution.

Where $\rho_r = \rho_f/\rho_m$ is the ratio of nanotube to matrix density. It is worth noting that $V_f = V_f^*$ corresponds to the uniformly distributed CNTR annular plate referred to as CNTR-UD. With V_f^* defined in Eq. (28), both the CGCNTR plate and CNTR-UD plate have the same value of CNTs mass fraction. For type V, the top surface of the plate ($N_z = 0.5$) is CNT-rich, (Fig. 3).

As can be seen in Fig. 3, for type Λ, the distribution of CNTs reinforcements is inversed and the bottom surface of the plate ($\eta_z = -0.5$) is CNT-rich, referred to as CGCNTR-Λ. For type X, a mid-plane symmetric graded distribution of CNTs reinforcements is achieved and both top and bottom surfaces are CNT-rich, referred to as CGCNTR-X. For type ◊, the distribution of CNTs reinforcements is inversed and both top and bottom surfaces are CNT-poor, whereas the reference surface ($\eta_z = 0$) is CNT-rich, referred to as CGCNTR-◊.

3. Teoretical Formulations

The mechanical constitutive relations that relate the stresses to the strains are as follows [54]:

$$\sigma_{ij} = \lambda\varepsilon_{kk}\delta_{ij} + 2\mu\varepsilon_{ij} \tag{29}$$

Where λ and μ are the Lame constants, ε_{ij} is the infinitesimal strain tensor and δ_{ij} is the Kronecker delta. In the absence of body forces, the equations of motion are as follows:

$$\begin{aligned}
&\frac{\partial\sigma_r}{\partial r}+\frac{1}{r}\frac{\partial\tau_{r\theta}}{\partial\theta}+\frac{\partial\tau_{rz}}{\partial z}+\frac{\sigma_r-\sigma_\theta}{r}=\rho\frac{\partial^2 u_r}{\partial t^2},\\
&\frac{\partial\tau_{r\theta}}{\partial r}+\frac{1}{r}\frac{\partial\sigma_\theta}{\partial\theta}+\frac{\partial\tau_{\theta z}}{\partial z}+2\frac{\tau_{r\theta}}{r}=\rho\frac{\partial^2 u_\theta}{\partial t^2},\\
&\frac{\partial\tau_{rz}}{\partial r}+\frac{1}{r}\frac{\partial\tau_{\theta z}}{\partial\theta}+\frac{\partial\sigma_z}{\partial z}+\frac{\tau_{rz}}{r}=\rho\frac{\partial^2 u_z}{\partial t^2}
\end{aligned} \tag{30}$$

The infinitesimal strain tensor is related to the displacements as follows:

$$\begin{aligned}
&\varepsilon_r=\frac{\partial u_r}{\partial r},\varepsilon_\theta=\frac{u_r}{r}+\frac{1}{r}\frac{\partial u_\theta}{\partial\theta},\varepsilon_z=\frac{\partial u_z}{\partial z},\\
&\gamma_{\theta z}=\frac{\partial u_\theta}{\partial z}+\frac{1}{r}\frac{\partial u_z}{\partial\theta},\gamma_{rz}=\frac{\partial u_r}{\partial z}+\frac{\partial u_z}{\partial r},\\
&\gamma_{r\theta}=\frac{1}{r}\frac{\partial u_r}{\partial\theta}+\frac{\partial u_\theta}{\partial r}-\frac{u_\theta}{r}
\end{aligned} \tag{31}$$

Where u_r, u_θ and u_z are displacement components along the r, θ and z directions, respectively. Moreover, ε_r, ε_θ, ε_z, $\gamma_{\theta z}$, $\gamma_{r\theta}$ and γ_{rz} are strain components. Upon substitution Eq. (31) with (29) and then with (30), the following equations of motion are obtained in terms of displacement components:

$$c_{11}\frac{\partial^2 u_r}{\partial r^2}+c_{12}\left(-\frac{1}{r^2}\frac{\partial u_\theta}{\partial\theta}+\frac{1}{r}\frac{\partial^2 u_\theta}{\partial r\partial\theta}+\frac{1}{r}\frac{\partial u_r}{\partial r}-\frac{1}{r^2}u_r\right)$$
$$+c_{13}\frac{\partial^2 u_z}{\partial r\partial z}+\frac{\partial c_{11}}{\partial r}\frac{\partial u_r}{\partial r}+\frac{\partial c_{12}}{\partial r}(\frac{u_r}{r}+\frac{1}{r}\frac{\partial u_\theta}{\partial\theta})+\frac{\partial c_{13}}{\partial r}\frac{\partial u_z}{\partial z}+$$
$$\frac{c_{66}}{r}[\frac{\partial^2 u_\theta}{\partial\theta\partial r}+\frac{1}{r}\frac{\partial^2 u_r}{\partial\theta^2}-\frac{1}{r}\frac{\partial u_\theta}{\partial\theta}]+\frac{\partial c_{55}}{\partial z}\left(\frac{\partial u_r}{\partial z}+\frac{\partial u_z}{\partial r}\right)+$$
$$c_{55}\left(\frac{\partial^2 u_r}{\partial z^2}+\frac{\partial^2 u_z}{\partial z\,\partial r}\right)+\frac{1}{r}[c_{11}\frac{\partial u_r}{\partial r}+c_{12}(\frac{u_r}{r}+\frac{1}{r}\frac{\partial u_\theta}{\partial\theta})+$$
$$c_{13}\frac{\partial u_z}{\partial z}-c_{12}\frac{\partial u_r}{\partial r}-c_{22}(\frac{u_r}{r}+\frac{1}{r}\frac{\partial u_\theta}{\partial\theta})-c_{23}\frac{\partial u_z}{\partial z}]$$
$$=\rho\frac{\partial^2 u_r}{\partial t^2} \tag{32}$$

$$c_{66}(\frac{-1}{r^2}\frac{\partial u_r}{\partial\theta}+\frac{1}{r}\frac{\partial^2 u_r}{\partial r\partial\theta}+\frac{\partial^2 u_\theta}{\partial r^2}+\frac{u_\theta}{r^2}-\frac{1}{r}\frac{\partial u_\theta}{\partial r})+$$
$$\frac{\partial c_{66}}{\partial r}(\frac{1}{r}\frac{\partial u_r}{\partial\theta}+\frac{\partial u_\theta}{\partial r}-\frac{u_\theta}{r})+\frac{1}{r}(c_{12}\frac{\partial^2 u_r}{\partial\theta\partial r}+c_{22}(\frac{1}{r}$$
$$\frac{\partial u_r}{\partial\theta}+\frac{1}{r}\frac{\partial^2 u_\theta}{\partial\theta^2})+c_{23}\frac{\partial^2 u_z}{\partial\theta\partial z})+c_{44}(\frac{\partial^2 u_\theta}{\partial z^2}+\frac{1}{r}\frac{\partial^2 u_z}{\partial z\,\partial\theta}$$
$$)+\frac{\partial c_{44}}{\partial z}(\frac{\partial u_\theta}{\partial z}+\frac{1}{r}\frac{\partial u_z}{\partial\theta})+\frac{2c_{66}}{r}(\frac{1}{r}\frac{\partial u_r}{\partial\theta}+\frac{\partial u_\theta}{\partial r}-$$
$$\frac{u_\theta}{r})=\rho\frac{\partial^2 u_\theta}{\partial t^2} \tag{33}$$

$$c_{55}(\frac{\partial^2 u_r}{\partial r\partial z}+\frac{\partial^2 u_z}{\partial r^2})+\frac{\partial c_{55}}{\partial r}(\frac{\partial u_r}{\partial z}+\frac{\partial u_z}{\partial r})+\frac{c_{44}}{r}(\frac{\partial^2 u_\theta}{\partial\theta\partial z}$$
$$+\frac{1}{r}\frac{\partial^2 u_z}{\partial\theta^2})+c_{13}\frac{\partial^2 u_r}{\partial z\,\partial r}+c_{23}(\frac{1}{r}\frac{\partial u_r}{\partial z}+\frac{1}{r}\frac{\partial^2 u_\theta}{\partial\theta\partial z})+c_{33}$$
$$\frac{\partial^2 u_z}{\partial z^2}+\frac{\partial c_{13}}{\partial z}\frac{\partial u_r}{\partial r}+\frac{\partial c_{23}}{\partial z}(\frac{u_r}{r}+\frac{1}{r}\frac{\partial u_\theta}{\partial\theta})+\frac{\partial c_{33}}{\partial z}\frac{\partial u_z}{\partial z}$$
$$+\frac{c_{55}}{r}(\frac{\partial u_r}{\partial z}+\frac{\partial u_z}{\partial r})=\rho\frac{\partial^2 u_z}{\partial t^2} \tag{34}$$

Equations (32 and 33) represent the in-plane equations of motion along the *r* and *θ*-axes, respectively; and Eq. (34) is the transverse or out-of-plane equation of motion. The related boundary conditions at *z=-h/2* and *h/2* are as follows:

at z=-h/2:

$$\sigma_z=K_w u_z-K_g(\frac{\partial^2 u_z}{\partial r^2}+\frac{1}{r}\frac{\partial u_z}{\partial r}+\frac{1}{r^2}\frac{\partial^2 u_z}{\partial\theta^2})$$
$$\tau_{zr}=0,\quad \tau_{z\theta}=0 \tag{35}$$

at z=h/2:

$$\tau_{zr}=0,\quad \tau_{z\theta}=0,\quad \sigma_z=0 \tag{36}$$

Where σ_{ij} is the component of stress sor; K_w and K_g are Winkler and shearing layer elastic coefficients of the foundation. Different types of classical boundary conditions at the circular edges of the plate can be stated as

-Clamped(*r=b*) - Clamped(*r=a*): (37)

at *r=a*
$u_r=u_\theta=u_z=0$
at *r=b*
$u_r=u_\theta=u_z=0$

-Simply supported(*r=b*) - Clamped(*r=a*): (38)

at *r=b*
$u_\theta=u_z=\sigma_r=0$
at *r=a*
$u_r=u_\theta=u_z=0$

-Simply supported(*r=b*) - Clamped(*r=a*): (39)

at *r=a*
$u_r=u_\theta=u_z=0$
at *r=b*
$\sigma_r=\tau_{r\theta}=\tau_{rz}=0$

4. DQM Solution for Equations of Motion and Boundary Conditions

It is necessary to develop appropriate methods for investigating the mechanical responses of CGCNTR structures. But, due to the complexity of the problem, it is difficult to obtain the exact solution. In this paper, the Differential Quadrature Method (DQM) approach is used to solve the governing equations of CGCNTR annular plates.

One can compare DQM solution procedure with the other two widely used traditional methods for plate analysis, i.e., Rayleigh-Ritz method and FEM. The main difference between the DQM and the other methods is how the governing equations are discretized. In DQM the governing equations and boundary conditions are directly discretized, and thus the elements of stiffness and mass matrices are evaluated directly. But in Rayleigh-Ritz and FEMs, the weak form of the governing equations is developed and the boundary conditions are satisfied in the weak form. Generally, a larger number of integrals with increasing amount of differentiation should be done to arrive at the element matrices. Also, the number of degrees of freedom is increased for an acceptable accuracy.

The basic idea of the DQM is the derivative of a function, with respect to a space variable at a given sampling point, which is approximated as a weighted

linear sum of the sampling points in the domain of that variable. In order to illustrate the DQ approximation, a function $f(\xi,\eta)$ defined on a rectangular domain $0\le\xi\le a$ and $0\le\eta\le b$ is considered. The function values are known or desired on a grid of sampling points in the given domain. According to DQM method, the rth derivative of the function $f(\xi,\eta)$ is approximated as what follows:

$$\frac{\partial^r f(\xi,\eta)}{\partial\xi^r}\ \Big|=\sum_{m=1}^{N_\xi}A_{im}^{\xi(r)}f(\xi_m,\eta_j)=\sum_{m=1}^{N_\xi}A_{im}^{\xi(r)}f_{mj} \tag{40}$$

For i=1, 2,…, N_ξ and r =1,2,…, $N_\xi-1$

From this equation one can deduce that the important components of DQM approximations are the weighting coefficients $A_{ij}^{\xi(r)}$ and the choice of sampling points. In order to determine the weighting coefficients a set of test functions are used in Eq. (40). The weighting coefficients for the first-order derivatives in ξ- direction are thus determined as what follows [58]:

$$A_{ij}^{\xi}=\begin{cases}\dfrac{1}{a}\dfrac{M(\xi_i)}{(\xi_i-\xi_j)M(\xi_j)} & for\quad i\neq j\\ -\sum\limits_{\substack{j=1\\ i\neq j}}^{N_\xi}A_{ij}^{\xi} & for\quad i=j\end{cases};i,j=1,2,...,N_\xi \tag{41}$$

where

$$M(\xi_i)=\prod_{j=1,i\neq j}^{N_\xi}(\xi_i-\xi_j) \tag{42}$$

The weighting coefficients of the second-order derivative can be obtained as the matrix form [58]:

$$\left[B_{ij}^{\xi}\right]=\left[A_{ij}^{\xi}\right]\left[A_{ij}^{\xi}\right]=\left[A_{ij}^{\xi}\right]^2 \tag{43}$$

In a similar manner, the weighting coefficients for the η-direction can be obtained.

The natural and simplest choice of the grid points is equally spaced points in the direction of the coordinate axes of computational domain. It is demonstrated that non-uniform grid points give a better result with the same number of equally spaced grid points [58]. It is shown [59] that one of the best options for obtaining grid points is Chebyshev–Gauss–Lobatto quadrature points:

$$\begin{aligned}\frac{\xi_i}{a}&=\frac{1}{2}\left\{1-\cos\left[\frac{(i-1)\pi}{(N_\xi-1)}\right]\right\},\frac{\eta_j}{b}\\&=\frac{1}{2}\left\{1-\cos\left[\frac{(j-1)\pi}{(N_\eta-1)}\right]\right\}\end{aligned} \tag{44}$$

For i = 1, 2,..., N_ξ ; j = 1,2,..., N_η

Using the geometrical periodicity of the plate, the displacement components for the free vibration analysis are represented as the following:

$$\begin{aligned}u_r(r,\theta,z,t)&=u_{rm}(r,z)\cos(m\theta)e^{i\omega t}\\u_\theta(r,\theta,z,t)&=u_{\theta m}(r,z)\sin(m\theta)e^{i\omega t}\\u_z(r,\theta,z,t)&=u_{zm}(r,z)\cos(m\theta)e^{i\omega t}\end{aligned} \tag{45}$$

Where m (=0,1,..., ∞) is the circumferential wave number; ω is the natural frequency and i (= $\sqrt{-1}$) is the imaginary number. It is obvious that m=0 means axisymmetric vibration. At this stage the DQ rules are employed to discretize the free vibration equations and the related boundary conditions. Substituting the displacement components for Eq. (45) and then using the DQ rules for the spatial derivatives, the discretized form of the equations of motion at each domain grid point (r_j,z_k) with (j = 2,3,..., N_r-1) and (k =2,3,..., N_z-1) is obtained as Eq. (32):

$$\begin{aligned}&(c_{11})_{jk}\sum_{n=1}^{N_r}B_{jn}^{r}u_{rmnk}+(c_{12})_{jk}\left(\frac{-u_{rmnk}}{r_j^2}+\frac{1}{r_j}\sum_{n=1}^{N_r}A_{jn}^{r}u_{rmnk}\right.\\&\left.-\frac{m}{r_j^2}u_{\theta mnk}+\frac{m}{r_j}\sum_{n=1}^{N_r}A_{jn}^{r}u_{\theta mnk}\right)+(c_{13})_{jk}\sum_{n=1}^{N_r}\sum_{r=1}^{N_z}A_{jn}^{r}A_{kr}^{z}u_{zmnr}\\&+\left(\frac{\partial c_{11}}{\partial r}\right)_{jk}\sum_{n=1}^{N_r}A_{jn}^{r}u_{rmnk}+\left(\frac{\partial c_{11}}{\partial r}\right)_{jk}\left(\frac{u_{rmjk}}{r_j}+\frac{m}{r_j}u_{\theta mjk}\right)\\&+\left(\frac{\partial c_{13}}{\partial r}\right)_{jk}\sum_{n=1}^{N_z}A_{kn}^{z}u_{zmjn}+\frac{(c_{66})_{jk}}{r_j}\left(\frac{-m^2}{r_j}u_{rmjk}\right.\\&\left.+m\sum_{n=1}^{N_r}A_{jn}^{r}u_{\theta mnk}-\frac{m}{r_j}u_{\theta mjk}\right)+(c_{55})_{jk}\left(\sum_{n=1}^{N_z}B_{kn}^{z}u_{rmjn}\right.\\&\left.+\sum_{n=1}^{N_r}\sum_{r=1}^{N_z}A_{jn}^{r}A_{kr}^{z}u_{zmnr}\right)+\left(\frac{\partial c_{55}}{\partial z}\right)_{jk}\left(\sum_{n=1}^{N_z}A_{kn}^{z}u_{rmjn}\right.\\&\left.+\sum_{n=1}^{N_r}A_{jn}^{r}u_{zmnk}\right)+\frac{1}{r_j}\left((c_{11})_{jk}\sum_{n=1}^{N_r}A_{jn}^{r}u_{rmnk}(c_{12})_{jk}\left(\frac{1}{r_j}u_{rmjk}\right.\right.\\&\left.\left.+\frac{m}{r_j}u_{\theta mjk}\right)+(c_{13})_{jk}\sum_{n=1}^{N_z}A_{kn}^{z}u_{zmjn}-(c_{12})_{jk}\sum_{n=1}^{N_r}A_{jn}^{r}u_{rmnk}\right.\\&\left.-(c_{22})_{jk}\left(\frac{1}{r_j}u_{rmjk}+\frac{m}{r_j}u_{\theta mjk}\right)-(c_{23})_{jk}\sum_{n=1}^{N_z}A_{kn}^{z}u_{zmjn}\right)\\&=-\omega^2\rho_{jk}u_{rmjk}\end{aligned} \tag{46}$$

Eq. (33):

$$\begin{aligned}&(c_{66})_{jk}\left(\frac{m}{r_j^2}u_{rmjk}-\frac{m}{r_j}\sum_{n=1}^{N_r}A_{jn}^{r}u_{rmnk}+\sum_{n=1}^{N_r}B_{jn}^{r}u_{\theta mnk}\right.\\&\left.+\frac{1}{r_j^2}u_{\theta mjk}-\frac{1}{r_j}\sum_{n=1}^{N_r}A_{jn}^{r}u_{\theta mnk}\right)+\left(\frac{\partial c_{66}}{\partial r}\right)_{jk}\left(\frac{-m}{r_j}u_{rmjk}\right.\\&\left.+\sum_{n=1}^{N_r}A_{jn}^{r}u_{\theta mnk}-\frac{1}{r_j}u_{\theta mjk}\right)+\frac{1}{r_j}\left((c_{12})_{jk}(-m)\sum_{n=1}^{N_r}A_{jn}^{r}u_{rmnk}\right.\\&\left.+(c_{22})_{jk}\left(\frac{m}{r_j}u_{rmjk}-\frac{m^2}{r_j}u_{\theta mjk}\right)+(c_{23})_{jk}(-m)\sum_{n=1}^{N_z}A_{kn}^{z}u_{zmjn}\right)\end{aligned}$$

$$-\frac{m^2}{r_j}u_{\theta mjk})+(c_{23})_{jk}(-m)\sum_{n=1}^{N_z}A_{kn}^{z}u_{zmjn})$$
$$+(c_{44})_{jk}(\sum_{n=1}^{N_z}B_{kn}^{z}u_{\theta mjn}-\frac{m}{r_j}\sum_{n=1}^{N_z}A_{kn}^{z}u_{zmjn})$$
$$+(\frac{\partial c_{44}}{\partial z})_{jk}(\sum_{n=1}^{N_z}A_{kn}^{z}u_{\theta mjn}-\frac{m}{r_j}u_{zmjk})+$$
$$\frac{2(c_{66})_{jk}}{r_j}(\frac{-m}{r_j}u_{rmjk}+\sum_{n=1}^{N_r}A_{jn}^{r}u_{\theta mnk}-\frac{1}{r_j}u_{\theta mjk})$$
$$=-\omega^2\rho_{jk}u_{\theta mjk} \quad (47)$$

Eq. (34):

$$(c_{55})_{jk}(\sum_{n=1}^{N_r}\sum_{r=1}^{N_z}A_{kr}^{z}A_{jn}^{r}u_{rmnr}+\sum_{n=1}^{N_r}B_{jn}^{r}u_{zmnk})$$
$$+(\frac{\partial c_{55}}{\partial r})_{jk}(\sum_{n=1}^{N_z}A_{kn}^{z}u_{rmjn}+\sum_{r=1}^{N_r}A_{jr}^{r}u_{zmrk})$$
$$+\frac{(c_{44})_{jk}}{r_j}(m\sum_{n=1}^{N_z}A_{kn}^{z}u_{\theta mjn}-\frac{m^2}{r_j}u_{zmjk})$$
$$+(c_{13})_{jk}(\sum_{n=1}^{N_r}\sum_{r=1}^{N_z}A_{kr}^{z}A_{jn}^{r}u_{rmnr})+(c_{23})_{jk}$$
$$(\frac{m}{r_j}\sum_{n=1}^{N_z}A_{kn}^{z}u_{\theta mjn}+\frac{1}{r_j}\sum_{n=1}^{N_z}A_{kn}^{z}u_{rmjn})$$
$$+(c_{33})_{jk}\sum_{n=1}^{N_z}B_{kn}^{z}u_{zmjn}+(\frac{\partial c_{13}}{\partial z})_{jk}\sum_{n=1}^{N_r}A_{jn}^{r}u_{rmnk}$$
$$+(\frac{\partial c_{23}}{\partial z})_{jk}(\frac{u_{rmjk}}{r_j}+\frac{m}{r_j}u_{\theta mjk})+(\frac{\partial c_{33}}{\partial z})_{jk}$$
$$\sum_{n=1}^{N_z}A_{kn}^{z}u_{zmjn}+\frac{(c_{55})_{jk}}{r_j}(\sum_{n=1}^{N_z}A_{kn}^{z}u_{rmjn}+\sum_{r=1}^{N_r}A_{jr}^{r}u_{zmrk})$$
$$=-\omega^2\rho_{jk}u_{zmjk} \quad (48)$$

Where A_{ij}^{r}, A_{ij}^{z} andB_{ij}^{r}, B_{ij}^{r} are the first-order and second-order DQ weighting coefficients in the r- and z-directions, respectively. In addition, U_{rmjk}, $U_{\theta mjk}$ and U_{zmjk} represent the displacement components of the node (j,k) defined by $r=r_j$ and $Z=Z_k$. Also, N_r and N_z represent the total number of nodes through the radial and thickness of the plate, respectively. In a similar manner the boundary conditions can be discretized. For this purpose, using Eq. (45) and the DQ discretization rules for spatial derivatives, the boundary conditions at *z = -h/2* and *h/2* , Eq. (35) become,

at z = *-h/2*

$$\sum_{n=1}^{N_z}A_{kn}^{z}u_{rmjn}+\sum_{n=1}^{N_r}A_{jn}^{r}u_{zmnk}=0,$$
$$\frac{-m}{r_j}u_{zmjk}+\sum_{n=1}^{N_z}A_{kn}^{z}u_{\theta mjn}=0,$$
$$(c_{13})_{jk}\sum_{n=1}^{N_r}A_{jn}^{r}u_{rmnk}+(c_{23})_{jk}(\frac{u_{rmjk}}{r_j}+\frac{m}{r_j}u_{\theta mjk})$$
$$+(c_{33})_{jk}\sum_{n=1}^{N_z}A_{kn}^{z}u_{zmjn}-K_{\omega}u_{zmjk}+K_g(\sum_{n=1}^{N_r}B_{jn}^{r}u_{zmnk}$$
$$+\frac{1}{r_j}\sum_{n=1}^{N_r}A_{jn}^{r}u_{zmnk}-\frac{m^2}{r_j^2}u_{zmjk})=0 \quad (49)$$

Eq. (36):

at z =*h/2*

$$\sum_{n=1}^{N_z}A_{kn}^{z}u_{rmjn}+\sum_{n=1}^{N_r}A_{jn}^{r}u_{zmnk}=0,$$
$$\frac{-m}{r_j}u_{zmjk}+\sum_{n=1}^{N_z}A_{kn}^{z}u_{\theta mjn}=0,$$
$$(c_{13})_{jk}\sum_{n=1}^{N_r}A_{jn}^{r}u_{rmnk}+(c_{23})_{jk}(\frac{u_{rmjk}}{r_j}$$
$$+\frac{m}{r_j}u_{\theta mjk})+(c_{33})_{jk}\sum_{n=1}^{N_z}A_{kn}^{z}u_{zmjn}=0 \quad (50)$$

Where k = 1 at z =*-h/2* and k =N_z at z =*h/2*, and *j* = 1, 2, . . ., N_r.

The boundary conditions at r = b and a state in equations (37-39) become,

Simply supported (S):

$$u_{\theta mjk}=0,u_{zmjk}=0,$$
$$(c_{11})_{jk}\sum_{n=1}^{N_r}A_{jn}^{r}u_{rmnk}+(c_{12})_{jk}(\frac{u_{rmjk}}{r_j}+$$
$$\frac{m}{r_j}u_{\theta mjk})+(c_{13})_{jk}\sum_{n=1}^{N_z}A_{kn}^{z}u_{zmjn}=0 \quad (51)$$

Clamped (C):

$$u_{rmjk}=0,\quad u_{\theta mjk}=0,\quad u_{zmjk}=0 \quad (52)$$

Free (F):

$$(c_{11})_{jk}\sum_{n=1}^{N_r}A_{jn}^{r}u_{rmnk}+(c_{12})_{jk}(\frac{u_{rmjk}}{r_j}+$$
$$\frac{m}{r_j}u_{\theta mjk})+(c_{13})_{jk}\sum_{n=1}^{N_z}A_{kn}^{z}u_{zmjn}=0,$$
$$\sum_{n=1}^{N_r}A_{jn}^{r}u_{\theta mnk}-\frac{m}{r_j}u_{rmjk}-\frac{1}{r_j}u_{\theta mjk}=0,$$
$$\sum_{n=1}^{N_z}A_{kn}^{z}u_{rmjn}+\sum_{n=1}^{N_r}A_{jn}^{r}u_{zmnk}=0 \quad (53)$$

In the above equations *k* = 2, . . ., N_z-1; also *j* = 1 at *r* = *b* and j = N_r at *r* = *a*. In order to carry out the eigenvalue analysis, the domain and boundary nodal displacements are separated. In vector forms, they are denoted as {d} and {b}, respectively. Based on this definition, the discretized form of the equations of motion and the related boundary conditions is represented in the matrix form as Equations of motion (46-48):

$$[[K_{db}][K_{dd}]]\begin{Bmatrix}\{b\}\\ \{d\}\end{Bmatrix}-\omega^2[M]\{d\}=\{0\} \quad (54)$$

Boundary conditions (49, 50) and (51-53):

$$\left[K_{bd}\right]\{d\}+\left[K_{bb}\right]\{b\}=\{0\} \tag{55}$$

Eliminating the boundary degrees of freedom in Eq. (54) using Eq. (55), this equation is obtained as follows:

$$\left[K\right]-\omega^2\left[M\right]\{d\}=\{0\} \tag{56}$$

Where $\left[K\right]=\left[K_{dd}\right]-\left[K_{db}\right]\left[K_{bb}\right]^{-1}\left[K_{bd}\right]$. The above eigenvalue system of equations can be solved to find the natural frequencies and mode shapes of the plate.

5. Numerical Results and Discussion

5.1. Convergence and Comparison Studies

Due to lack of appropriate results for free vibration of Continuously Graded Carbon Nanotube-Reinforced (CGCNTR) annular plates resting on a two-parameter foundation for direct comparison, validation of the presented formulation is conducted in two ways. Firstly, the results are compared with those of 1-D conventional functionally graded annular plates, and then, the results of the presented formulations are given in the form of convergence studies with respect to N_x and N_y, the number of discrete points distributed along the thickness and width of the plate, respectively.

As a first example, it is assumed that the material properties have the following exponential distributions in the thickness direction of the plate:

$$c_{ij}(z)=c_{ij}^{C}e^{(\frac{\lambda z}{h})},\rho(z)=\rho^{C}e^{(\frac{\lambda z}{h})} \tag{57}$$

Ceramic (Alumina, Al_2O_3):

$$E^{c}=380*10^{9}\,\mathrm{N/m^2},\rho^{c}=3{,}800Kg/m^3,\upsilon=0.3$$

Where the superscript C refers to the material properties of the bottom surface and λ is the material property graded index.

In Table 1, the first non-dimensional natural frequency parameters for the simply supported-clamped FG annular plates are compared with those of Nie and Zhong [35] and Dong [36].

As the second example, the first three non-dimensional frequencies for FG annular plates with clamped inner and outer edges for different circumferential wave number (m) are compared with those of the three-dimensional elasticity solution of Nie and Zhong [45] in Table 2.

As the third example, based on the power law distribution, the Young's modulus E and the mass density ρ are assumed to be in terms of a power law distribution as follows:

$$E(z)=E_C+E_{CM}V_f,\rho(z)=\rho_C+\rho_{CM}V_f \tag{58}$$

$$E_{CM}=E_M-E_C,\rho_{CM}=\rho_M-\rho_C,V_f=(\mathrm{z/h})^{g} \tag{59}$$

Where h is the thickness of the plate and g is the power law index which takes values greater than or equal to zero. Subscripts M and C refer to the metal and ceramic constituents which denote the material property of the top and bottom surface of the plate, respectively. The material properties are as follows:

$$E_M=70*10^{9}\,\mathrm{N/m^2},\upsilon=0.3,\rho_M=2702kg/m^3$$

Ceramic(Alumina, Al_2O_3):

$$E_C=380*10^{9}\,\mathrm{N/m^2},\upsilon=0.3,\rho_C=3800kg/m^3$$

In Tables 3 and 4, the results for FG annular plates are compared with those of Dong [36] for different values of the power law index and circumferential wave number (m). According to the data presented in the above-mentioned tables, excellent solution agreements are observed between the present method and those of the other methods.

Based on the above studies, a numerical value of $N_r = N_r = 17$ is used for the next studies.

After demonstrating the convergence and accuracy of the method, the results of parametric studies for 3-D vibration analysis of Continuously Graded Carbon Nanotube-Reinforced (CGCNTR) annular plates resting on an elastic foundation for different CNTs distributions and various thickness to outer radius ratio (h/a) and different combinations of free, simply supported and clamped boundary conditions at the circular edges, are computed. The non-dimensional natural frequency, Winkler and shearing layer elastic coefficients are as follows:

Table 1. Convergence results of the first non-dimensional natural frequency parameters $(\varpi = \omega h\sqrt{\rho / C_{11}}, C_{11} = E(1-\upsilon)/(1+\upsilon)(1-2\upsilon))$ for FG annular plates with simply supported (r=b) and clamped (r=a) edges $(a = 1m, b = 0.1, \mathrm{h/a} = 0.2)$

N_r=N_z	wave number (m)	λ			
		1	5	10	15
7	0	0.1886	0.1331	0.0784	0.0529
9		0.1873	0.1318	0.0783	0.0536
11		0.1872	0.1316	0.0782	0.0534
13		0.1872	0.1314	0.0782	0.0535
17		0.1870	0.1315	0.0781	0.0534
Ref. [36]		0.1871	0.1315	0.0780	0.0536
Ref. [35]		0.1936	-	-	-
7	1	0.1801	0.1313	0.0733	0.0475
9		0.1972	0.1394	0.0809	0.0576
11		0.1990	0.1401	0.0821	0.0579
13		0.1990	0.1401	0.0852	0.0581
17		0.1993	0.1402	0.0842	0.0582
Ref. [36]		0.1994	0.1402	0.0840	0.0582
Ref. [35]		0.2050	-	-	-
7	2	0.2744	0.1955	0.1227	0.0851
9		0.2748	0.1968	0.1202	0.0842
11		0.2785	0.1973	0.1201	0.0832
13		0.2783	0.1969	0.1201	0.0831
17		0.2782	0.1967	0.1187	0.0823
Ref. [36]		0.2781	0.1967	0.1184	0.0820
Ref. [35]		0.2684	-	-	-
7	3	0.3831	0.277	0.1715	0.1188
9		0.3824	0.2765	0.1697	0.1184
11		0.3824	0.2757	0.1696	0.1180
13		0.3819	0.2757	0.1692	0.1181
17		0.3819	0.2752	0.1692	0.1182
Ref. [36]		0.3819	0.2751	0.1693	0.1182
Ref. [35]		-	-	-	-

$$\Omega = \omega a^2\sqrt{\rho_m h/D_m}, D_m = E_m h^3/12(1-\upsilon_m^2) \quad (60)$$

$$K_g = k_g\, a^2/D_m, K_w = k_w\, a^4/D_m \quad (61)$$

where ρ_m, E_m and υ_m are mechanical properties of matrix. In this work, Poly (methyl methacrylate), referred to as PMMA, is selected for the matrix, and the material properties of which are assumed to be, $\upsilon_m = 0.34$ and $E_m = 2.5Gpa$ [60,61]. The (10,10) SWCNTs are selected as reinforcements. The material properties of the (10,10) SWCNTs used here from Refs. [17,60,61] are as follows (at room temperature, 300 K) :

$$E_f^{11} = 5.6466Tpa, E_f^{22} = 7.08Tpa,$$
$$G_f^{12} = 1.9445Tpa, \upsilon_f^{12} = 0.175$$

Table 2. Convergence results of the first three non-dimensional frequencies for FG annular plates with clamped - clamped edges $(a = 1m, b = 0.2m, h = 0.1m, \lambda = 1)$

wave number (m)	Number of the discrete points along the radial and thickness directions while using DQM						
	7	9	11	13	17	Ref.[45]	Ansys[1]
0	0.094	0.0856	0.0816	0.0801	0.0806	0.0807	0.0810
1	0.1006	0.0896	0.0844	0.0831	0.0838	0.0837	0.0839
2	0.1147	0.1027	0.0977	0.0955	0.0961	0.0961	0.0963

1. Ref. [45]

Table 3. Convergence study of the first five non-dimensional natural frequency parameters $(\varpi = \omega a\sqrt{\rho / G_m})$ for free vibration of a clamped-clamped FG annular plate.

N_r=N_z	wave number (m)	ϖ_1	ϖ_2	ϖ_3	ϖ_4	ϖ_5
7		8.177	13.912	15.516	19.446	20.108
9		8.201	13.875	15.511	19.481	20.158
11		8.208	13.867	15.511	19.484	20.162
13	0	8.210	13.870	15.511	19.485	20.164
17		8.213	13.872	15.515	19.485	20.166
Ref. [36]		8.214	13.872	15.514	19.485	20.167
7		8.303	9.696	13.803	14.885	15.546
9		8.322	9.689	13.769	14.853	15.533
11		8.327	9.688	13.767	14.851	15.533
13	1	8.329	9.688	13.765	14.850	15.533
17		8.332	9.689	13.766	14.849	15.536
Ref. [36]		8.333	9.689	13.766	14.850	15.535
7		8.849	11.160	13.842	15.638	16.561
9		8.861	11.147	13.814	15.615	16.548
11		8.863	11.146	13.812	15.615	16.549
13	2	8.865	11.145	13.810	15.614	16.549
17		8.868	11.145	13.811	15.614	16.550
Ref. [36]		8.869	11.145	13.810	15.615	16.550
7		9.901	12.693	14.423	16.390	17.699
9		9.906	12.681	14.399	16.422	17.714
11		9.919	12.670	14.402	16.451	17.718
13	3	9.921	12.673	14.407	16.453	17.720
17		9.923	12.673	14.407	16.456	17.721
Ref. [36]		9.924	12.672	14.407	16.455	17.721

$a/b=2.5, h/a=0.5, g=1$.

Table 4. Convergence study of the first five non-dimensional natural frequency parameters $(\varpi = \omega a\sqrt{\rho / G_m})$ for free vibration of a clamped-clamped FG annular plate.

N_r=N_z	wave number (m)	ϖ_1	ϖ_2	ϖ_3	ϖ_4	ϖ_5
7		10.063	18.379	19.726	24.456	25.726
9		10.087	18.342	19.720	24.421	25.786
11		10.094	18.333	19.721	24.424	25.790
13	0	10.096	18.336	19.721	24.425	25.792
17		10.098	18.338	19.723	24.427	25.794
Ref. [36]		10.099	18.338	19.724	24.426	25.794
7		10.237	12.343	18.229	18.615	19.676
9		10.256	12.336	18.195	18.583	19.653
11		10.261	12.335	18.193	18.580	19.649
13	1	10.263	12.335	18.191	18.578	19.649
17		10.267	12.336	18.191	18.579	19.651
Ref. [36]		10.266	12.336	18.192	18.578	19.651
7		10.917	14.407	18.479	18.514	20.715
9		10.929	14.394	18.451	18.490	20.702
11		10.931	14.393	18.449	19.490	20.703
13	2	10.933	14.392	18.447	19.489	20.703
17		10.936	14.392	18.448	19.489	20.704
Ref. [36]		10.937	14.392	18.448	19.490	20.704
7		12.178	16.685	19.325	20.630	22.402
9		12.228	16.673	19.301	20.662	22.413
11		12.241	16.662	19.304	20.691	22.418
13	3	12.243	16.665	19.309	20.693	22.420
17		12.247	16.664	19.310	20.694	22.421
Ref. [36]		12.246	16.664	19.310	20.695	22.421

$a/b=2.5, h/a=0.5, g=5$.

5.2. Parametric Studies

After demonstrating the convergence and accuracy of the method, the results of parametric studies for 3D vibration analysis of elastically supported thick CGCNTR annular plates reinforced by oriented CNTs for different CNTs distributions and various inner-to-outer radius ratio (b/a) and different combinations of free, simply supported, and clamped boundary conditions at the circular edges, are computed. Figures 4, 5 and 6 show the effect of the CNTs volume fraction V_f^* on CGCNTR-V to CNTR-UD fundamental frequency ratio, $\Omega_{11}^{CG}/\Omega_{11}^{UD}$, of the nanocomposite annular plates for different values of a/h ratio and boundary condtions including Clamped-Clamped, Simply Supported-Clamped, and Free-Clamped at the circular edges. Three different values of the CNTs volume fraction $V_f^* = 0.12, 0.17$ and 0.28 are taken into account. Correspondingly, the CNTs mass fractions are $m_f = 0.142, 0.2$ and 0.321, respectively, by taking the density of CNT $\rho_f = 1.4\, g/cm^3$ and the density of matrix $\rho_m = 1.15\, g/cm^3$ in Eq. (28). It can be seen that the discrepancies between the frequencies for the plates with continuously graded and uniform distribution of CNTs increase with the increase in the CNTs volume fraction V_f^*. This figure also shows/In this figure,it is also shown that the discrepancies between the frequencies decrease with the increase in the a/h ratio.

The variation of $\Omega_{11}^{CG}/\Omega_{11}^{UD}$ ratio of the nanocomposite annular plates with b/a and h/a ratios is shown in Figures 7, 8 and 9. As it is observed, the$\Omega_{11}^{CG}/\Omega_{11}^{UD}$ ratio decreases rapidly with the increase in b/a ratio and then remains almost unaltered for the b/a>7.

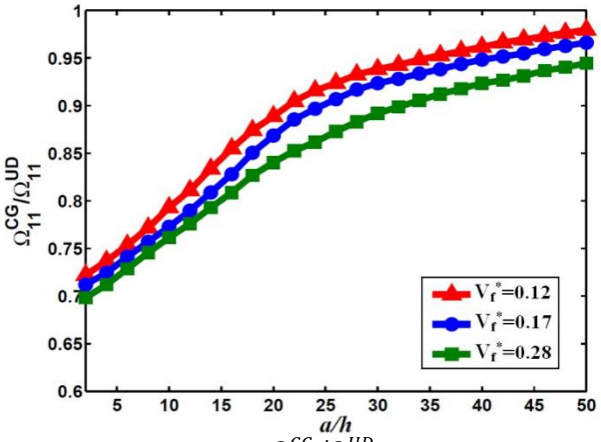

Figure 4. Variation of the $\Omega_{11}^{CG}/\Omega_{11}^{UD}$ ratio of the Clamped-Clamped nanocomposite annular plates resting on a two-parameter elastic foundation for different values of a/h ratio and CNTs volume fraction (Kg=10, Kw=100, b/a=0.4)

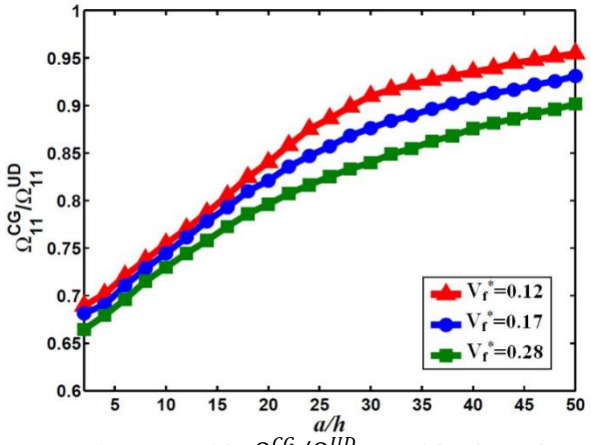

Figure 5. Variation of the $\Omega_{11}^{CG}/\Omega_{11}^{UD}$ ratio of the Clamped-Simply supported nanocomposite annular plates resting on a two-parameter elastic foundation for different values of a/h ratio and CNTs volume fraction (Kg=10, Kw=100, b/a=0.4)

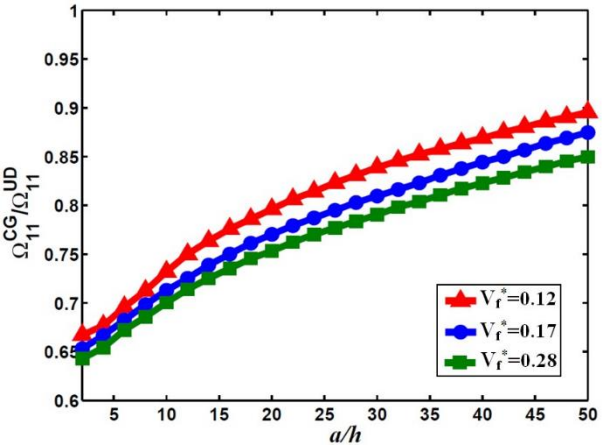

Figure 6. Variation of the $\Omega_{11}^{CG}/\Omega_{11}^{UD}$ ratio of the Clamped-Free nanocomposite annular plates resting on a two-parameter elastic foundation for different values of a/h ratio and CNTs volume fraction (Kg=10, Kw=100, b/a=0.4)

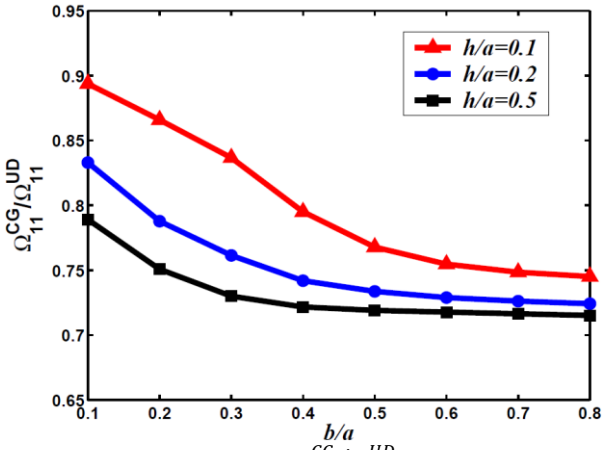

Figure 7. Variation of the $\Omega_{11}^{CG}/\Omega_{11}^{UD}$ ratio of the Clamped-Clamped nanocomposite annular plates resting on a two-parameter elastic foundation for different values of b/a and h/a ratios (Kg=10, Kw=100, Vf*=0.12)

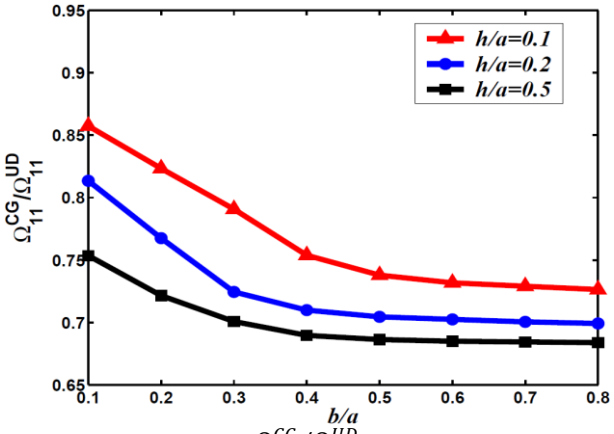

Figure 8. Variation of the $\Omega_{11}^{CG}/\Omega_{11}^{UD}$ ratio of the Clamped-Simply supported nanocomposite annular plates resting on a two-parameter elastic foundation for different values of b/a and h/a ratios (Kg=10, Kw=100, Vf*=0.12)

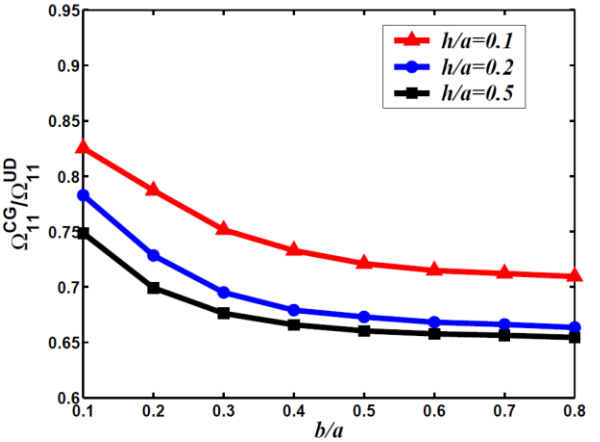

Figure 9. Variation of the $\Omega_{11}^{CG}/\Omega_{11}^{UD}$ ratio of the Clamped-Free nanocomposite annular plates resting on a two-parameter elastic foundation for different values of b/a and h/a ratios (Kg=10, Kw=100, Vf*=0.12)

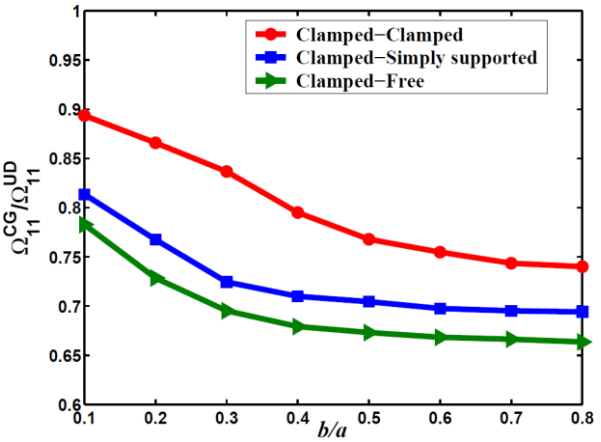

Figure 10. Variation of the $\Omega_{11}^{CG}/\Omega_{11}^{UD}$e ratio of the nanocomposite annular plates resting on a two-parameter elastic foundation for different boundary conditions and different values of b/a ratio (Kg=10, Kw=100, Vf*=0.12, h/a=0.2)

It is also observed that when the h/a ratio becomes bigger, the discrepancies between the frequencies for CGCNTR-V and CNTR-UD annualr plates become larger. In Fig. 10, the effect of various boundary conditions on the $\Omega_{11}^{CG}/\Omega_{11}^{UD}$ ratio of the nanocomposite annular plates with $V_f^* = 0.12$ for different values of b/a ratio is depicted. It can also be inferred from Fig. 10 that the Clamped-Clamped CGCNTR annular plate has the highest , whereas the Free-Clamped one has the lowest $\Omega_{11}^{CG}/\Omega_{11}^{UD}$ ratio values, implying that the discrepancies between the frequencies of CGCNTR and CNTR-UD annular plate with greater supporting rigidity are lower.In addition, Fig. 10 reveals that effects of the boundary conditions on the $\Omega_{11}^{CG}/\Omega_{11}^{UD}$ ratio diminish as b/a ratio increases.

In Fig. 11 the effects of variation of wave number (m) on the frequency parameters of Clamped-Clamped CGCNTR-V annular plate with $V_f^* = 0.12$ for different values of a/h ratio are demonstrated. According to Fig. 11, the general behavior of the frequency parameters of CGCNTR annular plate for all a/h ratios is that the frequency parameters converge only in the range beyond that of the fundamental frequency parameters. This means that the effects of a/h ratio are more prominent at low wave numbers, particularly those in the range beyond that of the fundamental frequency parameters, rather than at high wave numbers. As it is shown in Fig. 11, when the wave number increases the discrepancies between the frequency parameters for the different values of a/h ratio become larger. This behavior is also observed at other boundary conditions that again are not shown here for the sake of brevity. Fig. 12 shows the effects of variation of the Winkler elastic coefficient on the fundamental frequency parameters of the Clamped-Clamped nanocomposite annular plate and on different values of shearing layer elastic coefficient. It is clear that with increasing the elastic coefficients of the foundation, the frequency parameters increase to some limited values. It is observed for the large values of Winkler elastic coefficient, the shearing layer elastic coefficient has less effect and the results become independent of it. The influence of shearing layer elastic coefficient on the fundamental frequency parameters is shown in Fig. 13. One can see that the Winkler elastic coefficient has little effect on the fundamental frequency parameters at different values of shearing layer elastic coefficient. This behavior is also observed at other boundary conditions, but, for the sake of brevity, only this type of the boundary condition is considered.

In Fig. 11 the effects of variation of wave number (m) on the frequency parameters of Clamped-Clamped CGCNTR-V annular plate with $V_f^* = 0.12$ for different values of a/h ratio are demonstrated. According to Fig. 11, the general behavior of the fre-

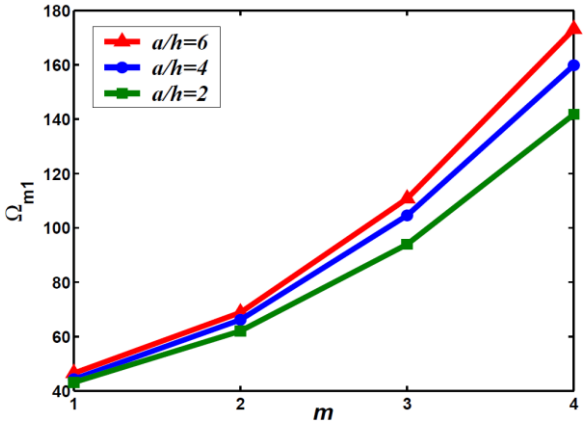

Figure 11. Variation of the circumferential wave number (m) of the Clamped-Clamped nanocomposite annular plates resting on a two-parameter elastic foundation for different values of a/h ratio (Kg=10, Kw=100, Vf^*=0.12, b/a=0.4)

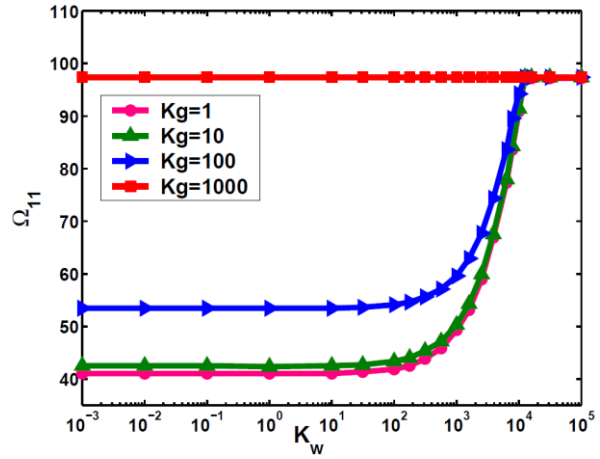

Figure 12. Variations of fundamental frequency parameters of the Clamped-Clamped nanocomposite annular plate resting on a two-parameter elastic foundation with Winkler and different shearing layer elastic coefficients (a/h=2, Vf^*=0.12, b/a=0.4)

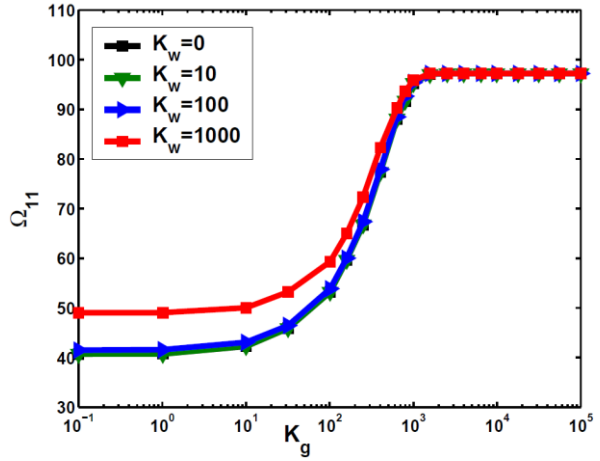

Figure 13. Variations of fundamental frequency parameters of the Clamped-Clamped nanocomposite annular plate versus the shearing layer elastic coefficient for different Winkler elastic coefficients (a/h=2, Vf^*=0.12, b/a=0.4)

quency parameters of CGCNTR annular plate for all a/h ratios is that the frequency parameters converge only in the range beyond that of the fundamental frequency parameters. This means that the effects of a/h ratio are more prominent at low wave numbers, particularly those in the range beyond that of the fundamental frequency parameters, rather than at high wave numbers. As it is shown in Fig. 11, when the wave number increases the discrepancies between the frequency parameters for the different values of a/h ratio become larger. This behavior is also observed at other boundary conditions that again are not shown here for the sake of brevity. Fig. 12 shows the effects of variation of the Winkler elastic coefficient on the fundamental frequency parameters of the Clamped-Clamped nanocomposite annular plate and on different values of shearing layer elastic coefficient. It is clear that with increasing the elastic coefficients of the foundation, the frequency parameters increase to some limited values. It is observed for the large values of Winkler elastic coefficient, the shearing layer elastic coefficient has less effect and the results become independent of it. The influence of shearing layer elastic coefficient on the fundamental frequency parameters is shown in Fig. 13. One can see that the Winkler elastic coefficient has little effect on the fundamental frequency parameters at different values of shearing layer elastic coefficient. This behavior is also observed at other boundary conditions, but, for the sake of brevity, only this type of the boundary condition is considered.

6. Conclusion Remarks

In the present work, differential quadrature method is employed to obtain a highly accurate semi-analytical solution for free vibration of nanocomposite annular plates resting on a two-parameter elastic foundation under various boundary conditions. The study is carried out based on the three-dimensional, linear and small strain elasticity theory. The volume fractions of oriented, straight Single-Walled Carbon Nanotubes (SWCNTs) are assumed to be graded in the thickness direction. The Eshelby-Mori-Tanaka approach is used to estimate the effective constitutive law of the elastic isotropic medium (matrix) with oriented, straight CNTs. The impacts of the volume fractions of oriented CNTs, different CNTs distributions, geometrical parameters and elastic coefficients of foundation on the vibrational characteristics of elastically supported thick annular plates are investigated. The following conclusions can be made from this study:

- Based on the achieved results, the continuously graded CNTs volume fractions can be utilized for the management of vibrational behavior of structures so that the frequency

parameters of structures made of such material can be considerably improved rather than the nanocomposites reinforced with uniformly distributed CNTs.

- The discrepancies between the frequencies for the plates with continuously graded and uniformly distributed CNTs decrease with an increase in the a/h ratio, but increase with an increase in the CNTs volume fraction V_f^*.
- The discrepancies between the natural frequencies of the continuously graded and uniformly distributed CNTs annular plate with greater supporting rigidity are lower.
- It is shown that the uniform distribution of CNTs volume fractions has the higher frequencies than that of asymmetric distributions, CGCNTR-Λ and CGCNTR-V.
- It is shown that with increasing the elastic coefficients of the foundation, the fundamental frequency parameters increase to some limited values. It is observed for the large values of Winkler elastic coefficient, the shearing layer elastic coefficient has less effect and the results become independent of it.
- It is shown that the variation of Winkler elastic coefficient has little effect on the fundamental frequency parameters at different values of shearing layer elastic coefficient. It is clear that in all cases, with increasing the shearing layer elastic coefficient of the foundation, the frequency parameters increase to some limited values. It is observed for the large values of shearing layer elastic coefficient; the results become independent of it.

Refferences

[1] Esawi AMK and Farag MM. Carbon nanotube reinforced composites: potential and current challenges. Mater Des 2007; 28: 2394-2401.

[2] Salvetat D and Rubio A. Mechanical properties of carbon nanotubes: a fiber digest for beginners. Carbon 2002; 40: 1729-1734.

[3] Endo M, Hayashi T, Kim YA, Terrones M and Dresselhaus MS. Applications of carbon nanotubes in the twenty-first century. Phil Trans R SocLondA 2004; 362: 2223-2238.

[4] Wernik JM and Meguid SA. Multiscale modeling of the nonlinear response of nano-reinforced polymers. ActaMech 2011; 217: 1-16.

[5] Thostenson ET, Ren ZF and Chou TW. Advances in the Science and Technology of Carbon Nanotubes and their Composites. A Review Compos Sci Technol 2001; 61: 1899-1912.

[6] Moniruzzaman M and Winey KI. Polymer nanocomposites containing carbon nanotubes. Macromolecules 2006; 39: 5194-5205.

[7] Valter B, Ram MK and Nicolini C. Synthesis of multiwalled carbon nanotubes and poly (o-anisidine) nanocomposite material: fabrication and characterization od its langmuir-schaefer films, Langmuir. 2002; 18: 1535-1541.

[8] Qian D, Dickey EC, Andrews R and Rantell T. Load transfer and deformation mechanisms in carbon nanotube-polystyrene composites. ApplPhys Lett 2000; 76: 2868-2870.

[9] Yokozeki T, Iwahori Y and Ishiwata S. Matrix cracking behaviors in carbon fiber/epoxy laminates filled with cup-stacked carbon nanotubes (CSCNTs). Composites Part A 2007; 38: 917-924.

[10] Hu N, Fukunaga H, Lu C, Kameyama M and Yan B. Prediction of elastic properties of carbon nanotube reinforced composites. Proc R Soc A 2005; 461: 1685-1910.

[11] Fidelus JD, Wiesel E, Gojny FH, Schulte K and Wagner HD. Thermo-mechanical properties of randomly oriented carbon/epoxy nanocomposites. Composites Part A 2005; 36: 1555-1561.

[12] Bonnet P, Sireude D, Garnier B and Chauvet O. Thermal properties and percolation in carbon nanotube-polymer composites. Appl Phys 2007; 91: 2019-2030.

[13] Han Y and Elliott J. Molecular dynamics simulations of the elastic properties of polymer/carbon nanotube composites. Comput Mater Sci 2007; 39: 315-323.

[14] Odegard GM, Gates TS, Wise KE, Park C and Siochi EJ. Constitutive modelling of nanotube reinforced polymer composites. Compos SciTechnol 2003; 63: 1671-1687.

[15] Shen HS. Nonlinear bending of functionally graded carbon nanotube-reinforced composite plates in thermal environments. Compos Struct 2009; 91: 9-19.

[16] Shen HS and Zhu ZH. Buckling and postbucklingbehavior of functionally graded nanotube-reinforced composite plates in thermal environments. Comput Mater Continua 2010; 18: 155-182.

[17] Shen HS and Zhang CL. Thermal buckling and postbucklingbehavior of functionally graded carbon nanotube-reinforced composite plates. Mater Des 2010; 31: 3403-3411.

[18] Ke LL, Yang J and Kitipornchai S. Nonlinear free vibration of functionally graded carbon nanotube reinforced composite beams. Compos Struct2010; 92: 676-683.

[19] Xiang Y, Kitipornchai S and Liew KM. Buckling and vibration of thick laminates on Pasternak foundations. Eng Mech ASCE 1996; 122: 54-63.

[20] Xiang Y, Wang CM and Kitipornchai S. Exact vibration solution for initially stressed Mindlin plates on Pasternak foundations. Int J MechSci1994; 36: 311-316.

[21] Wang CM, Kitipornchai S and Xiang Y. Relationships between buckling loads of Kirchhoff, Mindlin, and Reddy polygonal plates. Eng Mech ASCE 1997; 123: 1134-1137.

[22] Gupta US, Lal R and Sagar R. Effect of an elastic foundation on axisymmetric vibrations of polar orthotropic Mindlin circular plates. Indian J Pure Appl Math 1994; 25: 1317-1326.

[23] Ju F and Lee HPKH. Free vibration of plates with stepped variations in thickness on non-homogeneous elastic foundations. Sound Vib 1995; 183: 533-545.

[24] Gupta US, Lal R and Jain SK. Effect of elastic foundation on axisymmetric vibrations of polar orthotropic circular plates of variable thickness. Sound Vib 1990; 139: 503-513.

[25] Gupta US and Ansari AH. Effect of elastic foundation on axisymmetric vibrations of polar orthotropic linearly tapered circular plates. Sound Vib 2002; 254: 411-426.

[26] Laura PAA and Gutierrez RH. Free vibrations of a solid circular plate of linearly varying thickness and attached to Winkler foundation. Sound Vib 1991; 144: 149-161.

[27] Matsunaga H. Free vibration and stability of functionally graded plates according to a 2D higher-order deformation theory. J Compos Struct 2008; 82: 499-512.

[28] Zhou D, Cheung YK, Lo SH and Au FTK. Three-dimensional vibration analysis of rectangular thick plates on Pasternak foundation. Int J Numer Methods Eng 2004; 59: 1313-1334.

[29] Matsunaga H. Vibration and stability of thick plates on elastic foundations. Eng Mech ASCE 2000; 126: 27-34.

[30] Tahouneh V and Yas MH. 3-D free vibration analysis of thick functionally graded annular sector plates on Pasternak elastic foundation via 2-D differential quadrature method. Acta Mech2012; 223: 1879-1897.

[31] Tahouneh V and Yas MH. Semi-analytical solution for three-dimensional vibration analysis of thick multi-directional functionally graded annular sector plates under various boundary conditions. J EngMech ASCE 2013; In Press.

[32] Tahouneh V., Yas M.H., Tourang H., Kabirian M. Semi-analytical solution for three- dimensional vibration of thick continuous grading fiber reinforced (CGFR) annular plates on Pasternak elastic foundations with arbitrary boundary conditions on their circularedges. Meccanica,2013,48:1313-1336.

[33] Tahouneh V. Free vibration analysis of thick CGFR annular sector plates resting on elastic foundations. Struct Eng Mech 2014, Vol. 50, No. 6, 773-796.

[34] Jam J. E., Kamarian S., Pourasghar A., Seidi J. Free Vibrations of Three-Parameter Functionally Graded Plates Resting on Pasternak Foundations, Solid Mechanics 2012, Vol. 4, No. 1, pp. 59-74 (IAU, Arak Branch-Iran)

[35] Nie GJ and Zhong Z. Semi-analytical solution for three-dimensional vibration of functionally graded circular plates. Comput Methods Appl Mech Eng 2007; 196: 4901-4910.

[36] Dong CY. Three-dimensional free vibration analysis of functionally graded annular plates using the Chebyshev–Ritz method. Mater Des 2008; 29: 1518-1525.

[37] Cheng ZQ and Batra RC. Exact correspondence between eigenvalues of membranes and functionally graded simply supported polygonal plates. Sound Vib 2000; 229: 879-895.

[38] Malekzadeh P. Three-dimensional free vibrations analysis of thick functionally graded plates on elastic foundations. Compos Struct 2008; 89: 367-373.

[39] Bellman R and Casti J. Differential quadrature and long term integration. Math Anal Appl1971; 34: 235-238.

[40] Liu FL and Liew KM. Free vibration analysis of Mindlin sector plates numerical solutions by differential quadrature method. Comput MethodsApplMechEng 1999; 177: 77–92.

[41] Liew KM and Liu FL. Differential quadrature method for vibration analysis of shear deformable annular sector plates. Sound Vib 2000; 230: 335-356.

[42] Wang X and Wang Y. Free vibration analyses of thin sector plates by the new version of differential quadrature method. Comput Methods ApplMechEng 2004; 193: 3957-3971.

[43] Liew KM, Han JB, Xiao ZM and Du H. Differential quadrature method for Mindlin plates on Winkler foundation. Int J MechSci 1996; 38: 405-421.

[44] Gupta US, Lal R and Sharma S. Vibration analysis of non-homogeneous circular plate of nonlinear thickness variation by differential quadrature method. Sound Vib 2006; 298: 892-906.

[45] Nie GJ and Zhong Z. Dynamic analysis of multidirectional functionally graded annular plates. Appl Math Model 2010; 34: 608-616.

[46] Shu C. Differential quadrature and its application in engineering. Springer, 2000; Berlin.

[47] Shi DL, Feng XQ, Huang YY, Hwang KC and Gao H. The effect of nanotube waviness and agglomeration on the elastic property of carbon nanotube-reinforced composites. Eng Mater Technol 2004; 126: 250-257.

[48] Mori T and Tanaka K. Average Stress in Matrix and Average Elastic Energy of Materials With-Misfitting Inclusions.ActaMetall 1973; 21: 571-574.

[49] Giordano S, Palla PL and Colombo L. Nonlinear elasticity of composite materials, Landau coefficients in dispersions of spherical and cylindrical inclusions. EurPhys J B 2009; 68: 89-101.

[50] Benveniste Y. A new approach to the application of Mori-Tanaka's theory in composite materials. Mech Mater 1987; 6: 147-157.

[51] Chen CH and Cheng CH. Effective elastic moduli of misoriented short-fiber composites. Int J Solids Struct 1996; 33: 2519-2539.

[52] Eshelby JD. The determination of the elastic field of an ellipsoidal inclusion, and related problems. Proc R Soc A 1957; 241: 376-396.

[53] Eshelby JD. The elastic field outside an ellipsoidal inclusion. Proc R Soc A 1959; 252: 561–569.

[54] Formica G, Lacarbonara W and Alessi R. Vibrations of carbon nanotube-reinforced composites. Sound Vib 2010; 329: 1875-1889.

[55] Mura T. Micromechanics of defects in solids. The Hague: MartinusNijhoff; 1982.

[56] Shen HS. Postbuckling of nanotube-reinforced composite cylindrical shells in thermal environments. Part I: Axially-loaded shells, Compos Struct2011; 93: 2096-2108.

[57] Fung YC and Tong P. Classical and Computational Solid Mechanics. World Scientific Publishing Co, Singapore, 2001.

[58] Bert CW and Malik M. Differential quadrature method in computational mechanics: a review. Appl Mech Rev 1996; 49: 1-28.

[59] Shu C and Wang CM. Treatment of mixed and non-uniform boundary conditions in GDQ vibration analysis of rectangular plates.EngStruct1999; 21: 125-134.

[60] Shen HS. Thermal buckling and postbuckling-behavior of functionally graded carbon nanotube reinforced composite cylindrical shells. Compos Part B: Engineering, Article in Press, doi:10.1016/j.compositesb.2011.10.004; 2011.

[61] Wang ZX and Shen HS. Nonlinear vibration of nanotube-reinforced composite plates in thermal environments. Comp Mater Sci 2011; 50: 2319-2330.